HHS Public Access

Author manuscript

J Magn Reson Imaging. Author manuscript; available in PMC 2018 October 16.

Published in final edited form as:

J Magn Reson Imaging. 2015 December ; 42(6): 1582–1591. doi:10.1002/jmri.24935.

OKN-007 Decreases Tumor Necrosis and Tumor Cell Proliferation and Increases Apoptosis in a Preclinical F98 Rat Glioma Model

Patricia Coutinho de Souza, DVM, MSc[1,2], **Krithika Balasubramanian, PhD**[1], **Charity Njoku, MSc**[1], **Natalyia Smith, PhD**[1], **David L. Gillespie, PhD**[3], **Andrea Schwager, PhD**[4], **Osama Abdullah, BSc**[5], **Jerry W. Ritchey, DVM, PhD**[2], **Kar-Ming Fung, MD, PhD**[6], **Debra Saunders**[1], **Randy L. Jensen, MD, PhD**[3,7], and **Rheal A. Towner, PhD**[1,2,6,*]

[1]Advanced Magnetic Resonance Center, Oklahoma Medical Research Foundation, Oklahoma City, Oklahoma, USA

[2]Department of Veterinary Pathobiology, College of Veterinary Medicine, Oklahoma State University, Stillwater, Oklahoma, USA

[3]Huntsman Cancer Institute, University of Utah, Salt Lake City, Utah, USA

[4]Interdepartmental Program in Neuroscience, University of Utah, Salt Lake City, Utah, USA

[5]Department of Bioengineering, University of Utah, Salt Lake City, Utah, USA

[6]Department of Pathology, Oklahoma University Health Science Center, Oklahoma City, Oklahoma, USA

[7]Departments of Neurosurgery, Radiation Oncology, Oncological Sciences, Clinical Neurosciences Center, University of Utah, Salt Lake City, Utah, USA

Abstract

Background: Glioblastoma is a malignant World Health Organization (WHO) grade IV glioma with a poor prognosis in humans. New therapeutics are desperately required. The nitrone OKN-007 (2,4-disulfophenyl-PBN) has demonstrated effective anti-glioma properties in several rodent models and is currently being used as a clinical investigational drug for recurrent gliomas. We assessed the regional effects of OKN-007 in the tumor necrotic core and non-necrotic tumor parenchyma.

Methods: An F98 rat glioma model was evaluated using proton magnetic resonance spectroscopy (^{1}H-MRS), diffusion-weighted imaging (DWI), morphological T2-weighted imaging (T2W) at 7 Tesla (30 cm-bore MRI), as well as immunohistochemistry and microarray assessments, at maximum tumor volumes (15–23 days following cell implantation in untreated (UT) tumors, and 18–35 days in OKN-007-treated tumors).

Results: ^{1}H-MRS data indicates that Lip0.9/Cho, Lip0.9/Cr, Lip1.3/Cho, and Lip1.3/Cr ratios are significantly decreased (all $P < 0.05$) in the OKN-007-treated group compared with UT F98

*Address reprint requests to: R.A.T., Advanced Magnetic Resonance Center, Oklahoma Medical Research Foundation (OMRF), 825 NE 13th Street, Oklahoma City, OK 73104. rheal-towner@omrf.org.

gliomas. The Cho/Cr ratio is also significantly decreased in the OKN-007-treated group compared with UT gliomas. In addition, the OKN-007-treated group demonstrates significantly lower ADC values in the necrotic tumor core and the nonnecrotic tumor parenchyma (both $P < 0.05$) compared with the UT group. There was also an increase in apoptosis following OKN-007 treatment ($P < 0.01$) compared with UT.

Conclusion: OKN-007 reduces both necrosis and tumor cell proliferation, as well as seems to mediate multiple effects in different tumor regions (tumor necrotic core and nonnecrotic tumor parenchyma) in F98 gliomas, indicating the efficacy of OKN-007 as an anti-cancer agent and its potential clinical use.

Glioblastoma (GBM) IS the most common malignant and aggressive type of primary brain tumor in adults.[1] Most patients diagnosed with this tumor die within 1 year and only 5% survive more than 5 years despite aggressive therapies.[2] Advances in molecular biology of the tumor and tumor microenvironment have led to the development of novel therapies for GBMs; however, better therapeutic options are still needed to increase the prognosis of GBM patients.

The roles of nitrones, which include OKN-007 (OKlahoma Nitrone-007; 2,4-disulfophenyl-PBN), as anticancer agents in gliomas have been studied in detail.[3] OKN-007 is a small molecule that can traverse the blood–brain barrier, is anti-inflammatory, antioxidant, and proapoptotic.[3] In orthotopic rat F98 gliomas and human U87 xenografts, OKN-007 was found to significantly increase survival of treated versus untreated rats.[4–6] Morphological MRI showed that tumor volumes in both of these models were significantly decreased in treated compared with untreated (UT) animals.[5] Despite these findings, the effect of OKN-007 in different tumor regions are not fully understood, and the regional effect of OKN-007 on necrosis and cell proliferation has not been reported.

Proton magnetic resonance spectroscopy (^{1}H-MRS), used in research and clinical settings to measure brain metabolite levels, and diffusion-weighted imaging (DWI), used to characterize tumor growth by means of microscopic translational motion of water molecules within tissues, are among the most valuable techniques that can provide a more complete evaluation of functional, cellular, and metabolic information in human GBMs.[7]

Here, we report on the use of DWI and ^{1}H-MRS to assess the effects of OKN-007 on necrosis and cell proliferation in a F98 rat glioma model. Supporting histological and immunohistochemistry data for necrosis, cell proliferation and apoptosis, and microarray data analysis, are also presented.

Materials and Methods

Glioma Implantation

The animal studies were conducted with approval (100%) from the Institutional Animal Care and Use Committee. F98 rat glioma cell implantation was prepared as previously described.[5] F98 cells (10^5 in 10-μL volume) were intracerebrally implanted with a stereotaxic device (2 mm lateral and 2 mm anterior to the bregma at a 3-mm depth) in Fischer 344 rats (male 200–250 g). Animals were divided into two groups and assessed at

maximum tumor volumes: OKN-007-treated (18–35 days after cell implantation) and UT (15–23 days following cell implantation). Groups were stratified to ensure that tumor sizes were similar before initiation of treatment (11–15 days after cell implantation). For MR procedures rats were anesthetized (1.0–1.5% isoflurane). Not all animals were subjected to both MRS and DWI, which varied numbers for different datasets. Power calculations indicated that n≥9 rats per group allow detection of ~20% difference in tumor growth between treatment groups (95% confidence level). All animals were euthanized (CO_2 asphyxiation) at maximum tumor volumes.

OKN-007 Treatment

OKN-007 (Ryss Laboratories, Union City, CA) was administered to rats by drinking water (0.018% w/v). Treatment started at 15 days after glioma cell implantation, when tumor volumes were 10–15 mm^3, and was administered continuously until the end of the study. Rats receiving normal drinking water were used as UT controls. The amount of OKN-007 consumed by each rat housed in separate cages was determined by weighing water bottles each day. No significant deviation was observed in the volume of liquid uptake of compound in these rats (average intake of OKN-007 was ~10 mg/kg/day).

MRI

^{1}H-MR SPECTROSCOPY.—^{1}H-MRS values were obtained in UT (n = 14) and OKN-007-treated (n = 9) F98 gliomas, and 12 normal Fischer 344 rats. MRI experiments were conducted on a Bruker Biospec 7.0 Tesla (T) (Bruker Biospin, Germany), with a 72-mm quadrature volume coil for signal transmission and a rat head surface coil for signal reception, an actively shielded gradient set (max. 200 mT/m, 2 mT/m/A), and a water heater to maintain the body temperature at 37°C. Tumor morphology was observed on spin echo T2-weighted (T2W) images using rapid acquisition with relaxation enhancement (RARE), with TR (repetition time) = 5000 ms, effective TE (echo time) = 63 ms, 20 transverse 1-mm-thick slices, field of view = 3.5 × 3.5 cm^2, RARE factor = 8, in-plane resolution = 137 × 137 μm^2, and each scan taking 12 min 48 s.

^{1}H-MRS was acquired using stimulated-echo acquisition mode (STEAM), with TE5 4.4 ms, TM (mixing time) = 10 ms, TR = 3000 ms, 256 averages, and spectral width = 4006 Hz, and each scan taking 12 min 54 s. Nonsuppressed MR spectra were acquired beforehand by applying eddy-current correction to maximize signal intensity and decrease peak linewidths. Water was suppressed with variable power radio frequency pulses and optimized relaxation delays (VAPOR). For all cases, the peak width (full width at half maximum) of the water peak was less than 30 Hz following localized shimming (Fastmap, Bruker Biospin), conducted by using first- and second-order adjustments. Cubic voxels of 3.0 × 3.0 × 3.0 mm^3 were positioned in either tumor or contralateral normal brain tissue, while maximizing the amount of tumor tissue present in voxels at all times.

To analyze the MRS data, we used an in-house Mathematica (version 6.0, Wolfram Research, Champaign, IL) notebook. Spectra were then scaled in ppm by calibrating the water peak (4.78 ppm). Major brain metabolic peaks were identified as N-acetylaspartate (NAA) at 2.02 ppm, choline and choline-containing compounds (total Cho) at 3.22 ppm,

creatine (Cr) and phosphocreatine (referred to as total Cr) at 3.02 ppm, and mobile lipids (absent in the normal brain tissue), which appeared sharply at 1.3 ppm for the methylene group, and 0.9 ppm for the methyl group on fatty acyl groups, in tumor tissue. Quantification of variations in metabolite levels were evaluated as peak area ratios of tumor metabolites to contralateral choline and creatine: Cr/Cho, NAA/Cho, Lip1.3 (methylene)/Cho, and Lip0.9 (methyl)/Cho, Cho/Cr, NAA/Cr, Lip1.3 /Cr, and Lip0.9/Cr.

DWI.—An axial multislice DWI sequence covering the entire tumor was performed using echo planar imaging (EPI) four-shots pulse sequence (single direction) with the following: repetition time/echo time (TR/TE) = 3750/51.1 ms, matrix size5 128 × 128, diffusion gradient duration = 4 ms, diffusion gradient separation = 14 ms, five b values (200, 500, 1000, 2000, and 3000 s/mm^2), 234 μm/pixel × 234 μm/pixel in-plane resolution, and each scan taking 4 min 15 s. Apparent diffusion coefficient (ADC) maps were generated from parametric images for diffusion using traces of b-matrix values (Paravision 5.0) for all slices where tumors were observed. Uniform circular regions of interest (ROIs) of 10.0 mm^2 were drawn in tumor parenchyma and necrotic core regions in each slice of each animal. ADCs (×10 ^{3} mm^2/s) of each ROI were recorded as mean ± standard deviation, and obtained for each tumor region. The number of ROIs for tumor parenchyma in UT (n = 12) and OKN-007-treated (n = 12) groups were >1600, and for tumor necrotic core in UT and OKN-007-treated groups were >500.

Quantification of Tumor Necrosis

Percent tumor necrosis in UT (n = 10) and OKN-007 (n = 8) treated animals was also calculated from T2W images. Tumor and necrotic volumes (mm^3) were measured by drawing freehand ROIs to measure areas and multiplied by slice thickness and number of slices where tumors and necrotic tumor cores were observed. Percent tumor necrosis was calculated as follows: (total necrotic tumor volume/total tumor volume) × 100.

Quantification of Tumor Cellularity

Tumor cellularity was calculated in one representative hematoxylin and eosin (H&E) - stained slide for animals from each group (UT and OKN-007-treated) using Aperio ScanScope Image Analysis. The number of tumor cells was counted in three 1-mm^2 ROIs for each H&E-stained slide. Areas adjacent to or within necrotic or inflammatory regions were excluded while counting tumor cellularity. The number of cells per mm^2 were determined.

Immunohistochemistry

To characterize tumor cell proliferation and apoptosis in both UT and OKN-007-treated groups, immunohistochemistry for Ki-67 (1:100 dilution, rabbit polyclonal, clone PA5-19462, Thermo Fisher Scientific, IL) and active/cleaved Caspase 3 (1:200 dilution, rabbit polyclonal, clone NB600-1235, Novus Biologicals, CO) were performed using an automated immunostainer (Leica, Bond-III, Leica, Buffalo Grove, IL), respectively.

Aperio ScanScope Image Analysis was used to determine Ki-67 labeling index (Ki-67 LI) and apoptotic index (AI). Areas with the highest number of labeled nuclei were identified.

Ki-67 LI and AI were determined by counting 1000 cells and expressing this as the number of labeled cells per 1000 cells [8] for each animal from both treated groups. Labeled cells adjacent to or within necrotic areas were excluded while counting Ki-67 LI and AI.

Statistical Analysis

Statistical analyses were performed using Graph Pad Prism 6 (Graph Pad, San Diego, CA). All P values < 0.05 were considered statistically significant. Peak area ratios [Cho/Cr, Cr/Cho, NAA/Cr, NAA/Cho, Lip1.3/Cr, Lip1.3/Cho, Lip0.9/Cr, and Lip0.9/Cho], ADC value, total percent necrosis, tumor cell density, Ki-67 LI, and AI were reported as means ± standard deviations. Student t-tests (independent-samples, two-tailed t-test) were used to assess the differences between means of normal, UT, and OKN-007-treated F98 glioma rats.

Results

OKN-007 Inhibited Tumor Necrosis in the F98 Rat Glioma Model

Representative MR spectra are shown in Figure 1. ^{1}H-MRS values were obtained in normal Fischer 344 rats, and in UT and OKN-007-treated rats bearing F98 gliomas. Figure 2 shows that the, Lip0.9/Cho (P = 0.024), Lip0.9/Cr (P = 0.024), Lip1.3/Cho (P = 0.027), and Lip1.3/Cr (P = 0.027) ratios were significantly lower in OKN-007-treated group than in the UT F98 gliomas at the end phase of tumor progression.

Histological assignment of tumor periphery and necrotic core regions are shown in Figure 3A (UT) and Figure 3B (OKN-007-treated). ADC maps (Fig. 4A,B) were generated from the images and used to determine the ADC value of the necrotic tumor core in each animal from each group. ADC values within the necrotic tumor core of OKN-007-treated rats were significantly lower than UT animals (P < 0.05), which were both significantly higher than normal brain (P < 0.0001 for both) (Fig. 4C).

Morphological T2W images were used to assess the percent necrosis per tumor volume in both groups, which was significantly higher (P < 0.01) in UT (20.08% ± 2.00, n = 10) compared with OKN-007-treated rats (11.96% ± 1.80, n = 7) (Fig. 5). Tumor volumes were 224.51 ± 91.87 for UT and 125.15 ± 69.24 for OKN-007-treated animals (P = 0.023).

Furthermore, a partial microarray pathway analysis of isolated RNA from UT and OKN-007-treated F98 gliomas shows downregulation of genes associated with calcium-channel regulation due to OKN-007 (Fig. 6). The matrix Gla protein (MGP) and microfibrillar-associated protein 4 (MFAP4), which are directly associated with calcium-channel regulation, were both down-regulated by OKN-007. MGP was down-regulated by a 3.16-fold change and MFAP4 was down-regulated by a 2.16-fold change as a result of OKN-007 treatment. Two other genes linked to calcium-channel regulation were down-regulated by OKN-007: fibronectin type III domain-containing 1 gene, which is associated with G-protein $\beta\gamma$, and ADAM metallopeptidase, which is associated with the tumor necrosis factor (TNF).

OKN-007 Inhibited Tumor Cell Proliferation in the F98 Rat Glioma Model

The Cho/Cr ($P = 0.033$) ratio obtained in ^{1}H-MRS data was significantly lower in OKN-007-treated compared with UT F98 gliomas (Fig. 2B). Tumor cell density (number of tumor cells/mm^2) was evaluated from H&E-stained tumor sections of both treatment groups. The OKN-007-treated group (7571 ± 251, n = 10) showed significantly lower ($P < 0.001$) cellularity compared with UT rats (8442 ± 139, n = 10) (Fig. 3). For DWI, the OKN-007-treated group showed significantly higher ($P < 0.05$) ADC values for the non-necrotic tumor parenchyma compared with UT rats (Fig. 4D).

Tumor cell proliferation was evaluated by means of immunoexpression of Ki-67, which was significantly lower ($P < 0.05$) in OKN-007-treated (53.25 ± 5.72; n = 6) versus UT animals (71.73 ± 5.31; n = 7) (Fig. 7A–C). OKN-007 increased apoptosis, where AI was significantly higher ($P < 0.01$) in OKN-007-treated (27.09 ± 2.25, n = 5) compared with UT rats (11.69 ± 3.38; n = 7) (Fig. 7D–F).

Discussion

The anti-cancer response to OKN-007 in F98 gliomas (decreased tumor volume and increased survival) was previously reported based on morphological (T2W) imaging, bioluminescence imaging, and immunohistochemistry assessments, along with survival data.[5] Assessment of treatment response using other MR parameters, such as ^{1}H-MRS, DWI, and perfusion rates, was reported in C6 glioma models,[4,9] however the use of a multi-parametric approach and regional evaluation, has not been previously reported for F98 gliomas, which are more aggressive than C6 gliomas.

In this study, we assessed the effect of OKN-007 in necrotic tumor core and nonnecrotic tumor parenchyma regions in heterogeneous regions of F98 gliomas. We demonstrated that OKN-007 inhibited both tumor necrosis and cell proliferation in F98 gliomas. ^{1}H-MRS data showed decreases in Lip1.3/Cr, Lip1.3/Cho, Lip0.9/Cr, and Lip0.9/Cho ratios for OKN-007-treated versus UT F98 rat gliomas, which may be associated with decreased necrosis.

The role of mobile lipids in cancer has been the subject of many excellent reviews and articles.[6,9–18] In brain tumors, the elevation of lipid levels usually correlates with necrosis,[10,13,19,20] and lipids are considered as important biomarkers in the diagnosis and monitoring of treatment response.[13]

Necrosis is a hallmark of GBMs,[21,22] with some studies suggesting it is present in over 85% of cases.[23–26] It is caused by tumor hypoxia as a result of increased cell proliferation and mitotic activity, as well as insufficient tissue perfusion.[22‘27] The pathway of necrosis in glioblastoma begins with acute cellular ATP depletion as a result of electron transport chain collapse and subsequent decreased oxidative phosphorylation.[28] This lack of ATP leads to a failure in the ATP-dependent ion channels and pumps, which initiates a massive cell volume increase through Na^+ influx. The increased intracellular Na^+ concentration results in activation of the Na^+-K^+-ATPase, which further depletes cellular ATP stores.[29] This depletion leads to the opening of nonselective Ca^{2+} channels, resulting in elevated intracellular Ca^{2+} levels and activation of the Ca^{2+}-ATPase with eventual mitochondrial

depolarization.[29] In addition, with severe ATP depletion, ionic homeostasis is no longer maintained by the K^+ efflux, leading to further Na^+ and water influxes that precipitate cellular swelling and collapse. As the cell membrane ruptures, the contents of the cells are released into the extracellular space, which will lead to the presence of high lipid peaks that are detected in ^{1}H-MRS.

In our study, we also found that the AI was higher in OKN-007-treated rats compared with UT animals, indicating OKN-007 also affects apoptosis. Abnormal cell survival and resistance to apoptosis is also thought to result in central necrosis, a characteristic feature of glioblastoma.[30] The propensity of glioblastoma for necrosis is also due, in part, to its resistance to apoptosis, which drives cells to necrosis as an alternative method of cell death.[30]

Spectroscopic findings were also confirmed by DWI and histopathological data analyses. We effectively showed that ADC values within the necrotic tumor core of OKN-007-treated animals were lower than those in UT rats. The inhibitory effect of OKN-007 in the necrotic tumor core of F98 gliomas was also noted in T2W images from each treatment group. Percent necrosis tumor volumes were lower in OKN-007-treated compared with UT rats. A possible explanation for this observation could be that OKN-007 affects necrosis by down-regulating the genes associated with Ca^{2+} channels, thereby reducing intracellular Ca^{2+} levels. The effect of OKN-007 on genes associated with Ca^{2+} channels was confirmed by microarray, where OKN-007 was shown to down-regulate two genes, MGP and MFAP4, which are directly related to Ca^{2+} channels. In addition, a few other genes associated with Ca^{2+} channels also seem to be down-regulated by OKN-007. Because TNFa is related to the genes associated with Ca^{2+} channels, down-regulation of Ca^{2+}-related genes could also lead to reduced expression of genes for TNFα, which in turn down-regulates the *NF-κβ* pathway, thereby causing a decrease in necrosis. There was also down-regulation of ADAMTS8, which is directly linked to TNF.

Furthermore, our study also demonstrated that OKN-007 inhibited tumor cell proliferation in F98 rat gliomas. Previous studies have confirmed that the relative increase in choline in most high-grade gliomas is due to an increase in membrane synthesis and accelerated cell proliferation.[31,32] Total Cho is a composite peak with contributions from choline, phosphocholine, and glycerophosphocholine. An increase in total Cho in tumors arises primarily from the synthesis and accumulation of phosphocholine, a metabolite produced by the rapid uptake and phosphorylation of choline that is necessary for the downstream synthesis of phosphatidylcholine, a major membrane phospholipid constituting around 25% of mammalian cellular lipids.[33,34] We demonstrated that OKN-007 decreased the Cho/Cr ratio at the end phase of tumor progression, due to a decrease in tumor cell proliferation, which was also confirmed by DWI and histopathological results.

Both intra- and extracellular spaces and their exchange contribute to the measured ADC. As cellular density increases, the added tortuosity to extracellular mobility paths reduces water mobility and, consequently, the ADC value.[35] Based on that observation, within a given tissue or cell type, ADC is useful as an indicator of the relative cellularity, such as in the evolution of tumor over time following therapy.[36] ADC is inversely proportional to cell

density,[37] and after an effective treatment, cellularity is reduced from apoptosis and necrosis, and diffusivity increases.[38] A rise in ADC indicates a positive response to therapy. The observed increase in water ADC following therapy is directly related to the number of tumor cells killed and is thought to be due to the liberation of water into the extracellular space.[36] In our study, the ADC values in the nonnecrotic tumor parenchyma of OKN-treated animals were significantly higher than UT rats, reflecting less restricted diffusion consequent to a decrease in tumor cellularity in OKN-007-treated F98 gliomas.

Tumor cell density and cell proliferation were also evaluated using H&E-stained tumor sections and immunoexpression of the antibody anti-Ki-67, respectively. OKN-007-treated rats showed significantly lower cellularity compared with UT animals. Ki-67 LI was significantly lower in OKN-007-treated compared with UT rats. Our results also corroborated data from other studies,[39] confirming a positive correlation of the glioma Cho signal with cell density, and an inverse linear correlation between glioma cell density and ADC values.

Limitations associated with this study are that animals were evaluated at a final time-point, and longitudinal follow-up studies need to be done. Regarding ^{1}H-MRS, spectroscopic imaging to assess regional changes in tumor metabolism should be considered.

In conclusion, our ^{1}H-MRS, DWI, immunohistochemical, and microarray data analyses showed that OKN-007 reduced necrosis and tumor cell proliferation, which further supports the use of OKN-007 as a potential antiglioma agent. It was established that both ADC and spectroscopic choline measures are related to glioma cell density in F98 gliomas. Furthermore, OKN-007 mediates multiple effects on different (tumor necrotic core and nonnecrotic tumor parenchyma) regions of the tumor in F98 gliomas that can be detected in vivo.

Acknowledgments

Contract grant sponsor: the National Institute of General Medical Sciences of the National Institutes of Health; Contract grant number: P20 GM103639; Contract grant sponsor: Oklahoma Center for the Advancement of Science and Technology; Contract grant number: AR092-049; Contract grant sponsor: Huntsman Cancer Center; Contract grant number: P30CA042014.

We thank Dr. B. Frank for obtaining the microarray data, and Ms. K. Kraus for editing the manuscript. We thank the Peggy and Charles Stephenson Cancer Center at the University of Oklahoma, Oklahoma City, OK, for funding and received an Institutional Development Award (IDeA) from the National Institute of General Medical Sciences of the National Institutes of Health for the use of Histology and Immunohistochemistry Core for providing immunohistochemistry and photographic services. This work was also supported by Oklahoma Medical Research Foundation; Oklahoma Center for the Advancement of Science and Technology (to R.A.T.); and the Huntsman Cancer Center (from the National Cancer Institute to R.L.J.).

References

1. Furnari FB, Fenton T, Bachoo RM, et al. Malignant astrocytic glioma: genetics, biology, and paths to treatment. Genes Dev 2007;21:2683–2710. [PubMed: 17974913]
2. Central Brain Tumor Registry of the United States. CBTRUS statistical report: primary brain and central nervous system tumors diagnosed in the United States in 2004–2008. Hinsdale, IL: CBTRUS; 2012.
3. Floyd RA, Chandru HK, He T, Towner R. Anti-cancer activity of nitrones and observations on mechanism of action. Anticancer Agents Med Chem 2011;11:373–379. [PubMed: 21651461]

4. Garteiser P, Doblas S, Watanabe Y, et al. Multiparametric assessment of the anti-glioma properties of OKN007 by magnetic resonance imaging. J Magn Reson Imaging 2010;31:796–806. [PubMed: 20373422]
5. Towner RA, Gillespie DL, Schwager A, et al. Regression of glioma tumor growth in F98 and U87 rat glioma models by the nitrone OKN-007. NeuroOncol 2013;15:330–340.
6. He T, Doblas S, Saunders D, et al. Effects of PBN and OKN007 in rodent glioma models assessed by ^{1}H MR spectroscopy. Free Radic Biol Med 2011;51:490–502. [PubMed: 21600283]
7. Khayal IS, Crawford FW, Saraswathy S, et al. Relationship between choline and apparent diffusion coefficient in patients with gliomas. J Magn Reson Imaging 2008;27:718–725. [PubMed: 18383265]
8. Ralte AM, Sharma MC, Karak AK, Mehta VS, Sarkar C. Clinicopathological features, MIB-1 labeling index and apoptotic index in recurrent astrocytic tumors. Pathol Oncol Res 2001;7:267–278. [PubMed: 11882906]
9. Doblas S, He T, Saunders D, et al. In vivo characterization of several rodent glioma models by ^{1}H MRS. NMR Biomed 2012;25:685–694. [PubMed: 21954105]
10. Gillies RJ, Morse DL. In vivo magnetic resonance spectroscopy in cancer. Annu Rev Biomed Eng 2005;7:287–326. [PubMed: 16004573]
11. Zoula S, Hérigault G, Ziegler A, Farion R, Décorps M, Rémy C. Correlation between the occurrence of ^{1}H-MRS lipid signal, necrosis and lipid droplets during C6 rat glioma development. NMR Biomed 2003; 16:199–212. [PubMed: 14558118]
12. Blankenberg FG, Katsikis PD, Storrs RW, et al. Quantitative analysis of apoptotic cell death using proton nuclear magnetic resonance spectroscopy. Blood 1997;89:3778–3786. [PubMed: 9160684]
13. Delikatny EJ, Chawla S, Leung DJ, Poptani H. MR-visible lipids and the tumor microenvironment. NMR Biomed 2011;24:592–611. [PubMed: 21538631]
14. Li X, Vigneron DB, Cha S, et al. Relationship of MR-derived lactate, mobile lipids, and relative blood volume for gliomas in vivo. AJNR Am J Neuroradiol 2005;26:760–769. [PubMed: 15814918]
15. de Certaines JD, Le Moyec L, Sequin F, Eliat PA, Constans JM. Nuclear magnetic resonance spectroscopy of lipids in cancer. Curr Org Chem 2007;11:529–546.
16. Hakumäki JM, Kauppinen RA. 1H NMR visible lipids in the life and death of cells. Trends Biochem Sci 2000;25:357–362. [PubMed: 10916153]
17. Bulik M, Jancalek R, Vanicek J, Skoch A, Mechl M. Potential of MR spectroscopy for assessment of glioma grading. Clin Neurol Neurosurg 2013;115:146–153. [PubMed: 23237636]
18. Negendank W, Sauter R. Intratumoral lipids in 1H MRS in vivo in brain tumors: experience of the Siemens cooperative clinical trial. Anticancer Res 1996;16:1533–1538. [PubMed: 8694522]
19. Barba I, Cabañas ME, Arús C. The relationship between nuclear magnetic resonance-visible lipids, lipid droplets, and cell proliferation in cultured C6 cells. Cancer Res 1999;59:1861–1868. [PubMed: 10213493]
20. Kuesel AC, Sutherland GR, Halliday W, Smith IC. ^{1}H MRS of high grade astrocytomas: mobile lipid accumulation in necrotic tissue. NMR Biomed 1994;7:149–155. [PubMed: 8080717]
21. Louis DN, Ohgaki H, Wiestler OD, et al. The 2007 WHO classification of tumours of the central nervous system. Acta Neuropathol 2007; 114:97–109. [PubMed: 17618441]
22. Kao HW, Chiang SW, Chung HW, Tsai FY, Chen CY. Advanced MR imaging of gliomas: an update. Biomed Res Int 2013;2013:970586. [PubMed: 23862163]
23. Barker FG, Jr, Davis RL, Chang SM, Prados MD. Necrosis as a prognostic factor in glioblastoma multiforme. Cancer 1996;77:1161–1166. [PubMed: 8635139]
24. Homma T, Fukushima T, Vaccarella S, et al. Correlation among pathology, genotype, and patient outcomes in glioblastoma. J Neuropathol Exp Neurol 2006;65:846–854. [PubMed: 16957578]
25. Miller CR, Dunham CP, Scheithauer BW, Perry A. Significance of necrosis in grading of oligodendroglial neoplasms: a clinicopathologic and genetic study of newly diagnosed high-grade gliomas. J Clin Oncol 2006;24:5419–5426. [PubMed: 17135643]
26. Pierallini A, Bonamini M, Pantano P, et al. Radiological assessment of necrosis in glioblastoma: variability and prognostic value. Neuroradiology 1998;40:150–153. [PubMed: 9561517]

27. Yamasaki F, Takaba J, Ohtaki M, et al. Detection and differentiation of lactate and lipids by single-voxel proton MR spectroscopy. Neurosurg Rev 2005;28:267–277. [PubMed: 16133454]
28. Noch E, Khalili K. Molecular mechanisms of necrosis in glioblastoma: the role ofglutamate excitotoxicity. Cancer Biol Ther 2009;8:1791–1797. [PubMed: 19770591]
29. Padanilam BJ. Cell death induced by acute renal injury: a perspective on the contributions of apoptosis and necrosis. Am J Physiol Renal Physiol 2003;284:F608–F627. [PubMed: 12620919]
30. Belden CJ, Valdes PA, Ran C, et al. Genetics of glioblastoma: a window into its imaging and histopathologic variability. Radiographics 2011;31:1717–1740. [PubMed: 21997991]
31. Nelson SJ. Analysis of volume MRI and MR spectroscopic imaging data for the evaluation of patients with brain tumors. Magn Reson Med 2001;46:228–239. [PubMed: 11477625]
32. Matsumura A, Isobe T, Anno I, Takano S, Kawamura H. Correlation between choline and MIB-1 index in human gliomas. A quantitative in proton MR spectroscopy study. J Clin Neurosci 2005;12: 416–420. [PubMed: 15925772]
33. Glunde K, Jie C, Bhujwalla ZM. Molecular causes of the aberrant choline phospholipid metabolism in breast cancer. Cancer Res 2004;64: 4270–4276. [PubMed: 15205341]
34. Podo F Tumour phospholipid metabolism. NMR Biomed 1999;12: 413–439. [PubMed: 10654290]
35. Chenevert TL, Sundgren PC, Ross BD. Diffusion imaging: insight to cell status and cytoarchitecture. Neuroimaging Clin N Am 2006;16: 619–632. [PubMed: 17148023]
36. Chenevert TL, Stegman LD, Taylor JM, et al. Diffusion magnetic resonance imaging: an early surrogate marker of therapeutic efficacy in brain tumors. J Natl Cancer Inst 2000;92:2029–2036. [PubMed: 11121466]
37. Ellingson BM, Malkin MG, Rand SD, et al. Validation of functional diffusion maps (fDMs) as a biomarker for human glioma cellularity. J Magn Reson Imaging 2010;31:538–548. [PubMed: 20187195]
38. Koh DM, Collins DJ. Diffusion-weighted MRI in the body: applications and challenges in oncology. AJR Am J Roentgenol 2007;188:1622–1635. [PubMed: 17515386]
39. Gupta RK, Cloughesy TF, Sinha U, et al. Relationships between choline magnetic resonance spectroscopy, apparent diffusion coefficient and quantitative histopathology in human glioma. J Neurooncol 2000;50:215–226. [PubMed: 11263501]

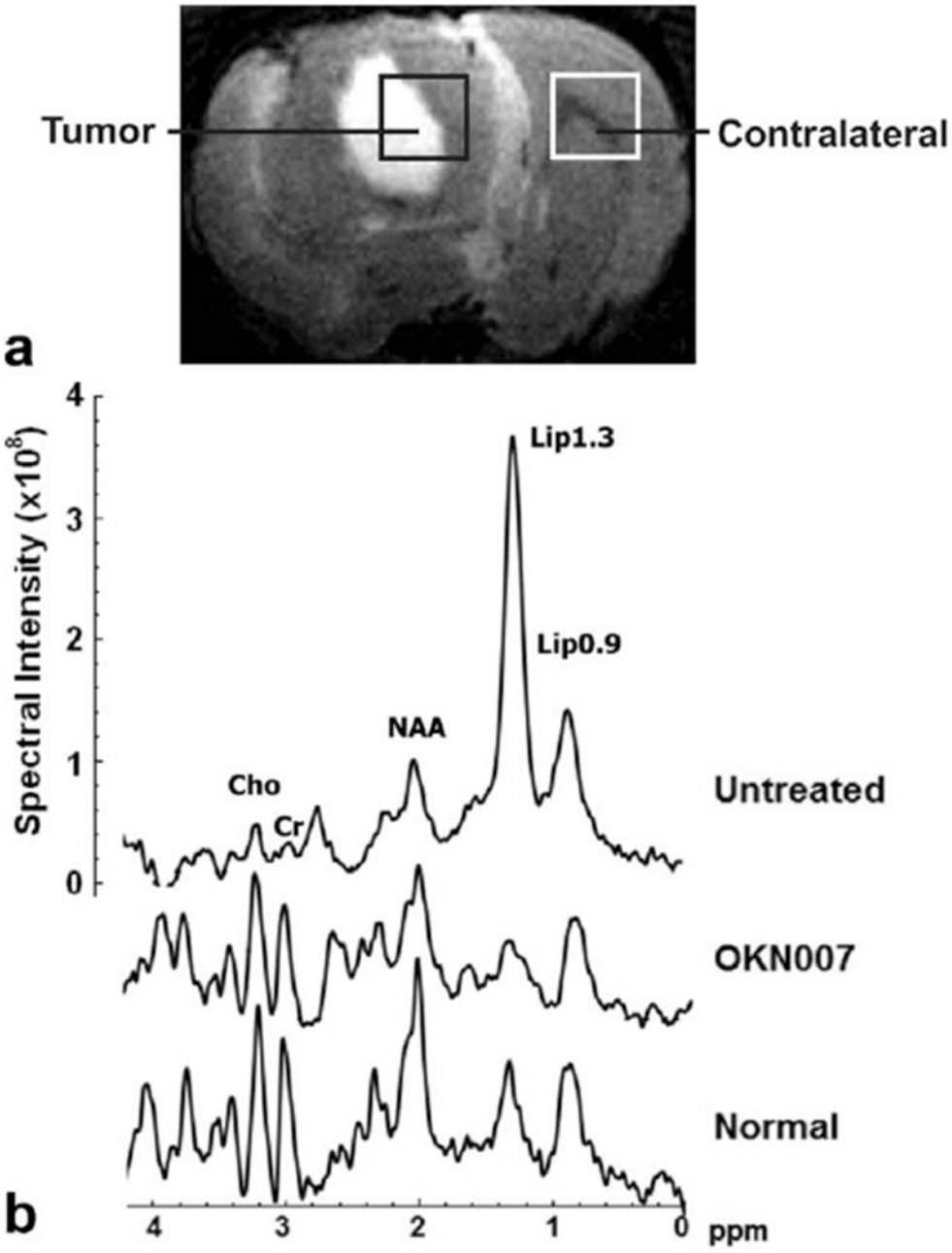

FIGURE 1:

Representative ^{1}H-MR spectra from untreated and OKN-007-treated F98 gliomas. **A:** Voxel ($3 \times 3 \times 3$ mm^3) location for ^{1}H-MR spectra in tumor and contralateral brain regions in an untreated F98 glioma. **B:** Representative ^{1}H-MR spectra from F98 gliomas depicting alterations in metabolite ratios from normal brain and OKN-007-treated and untreated (UT) glioma tissues. Spectra were obtained at the end-tumor growth phase. Spectral intensity for untreated tumor is the same for OKN-007and normal brain examples.

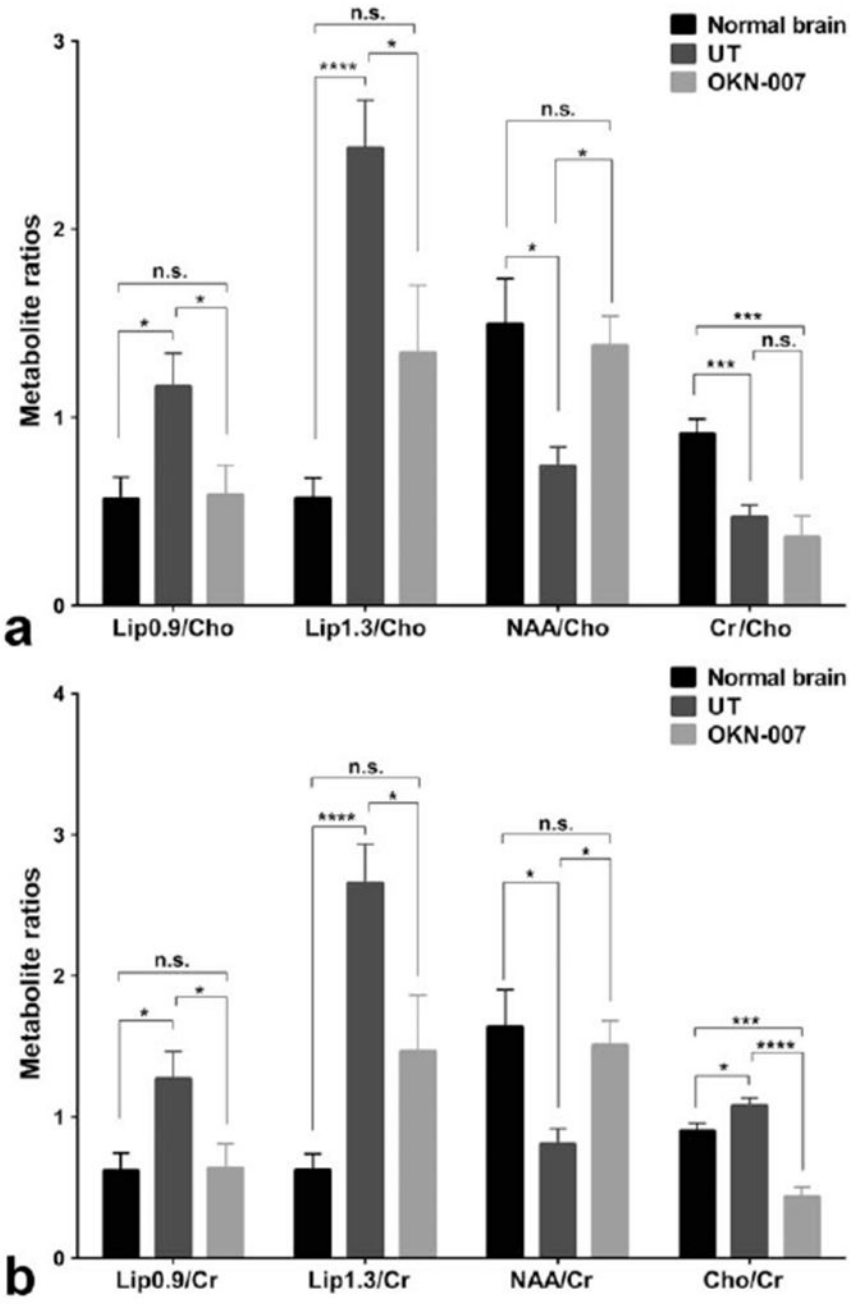

FIGURE 2:

OKN-007 affects tumor metabolites in F98 gliomas. Brain metabolite ratios in normal rat brain (n = 12) and UT (n = 14) and OKN-treated (n = 9) F98 rat gliomas compared with contralateral (normal) Cho (**A**) or Cr (**B**). UT group showed significantly higher Cho/Cr, Lip1.3/Cr, Lip1.3/Cho, Lip0.9/Cr, and Lip0.9/Cho compared with normal rat brain. Cho/Cr, Lip0.9/Cr, Lip0.9/Cho, Lip1.3/Cr, and Lip1.3/Cho ratios were significantly lower in OKN-007-treated group compared with untreated F98 gliomas at end phase of tumor growth. OKN-007-treated group demonstrated significantly lower Cho/Cr ratios compared

with normal rat brain. There was no significant difference between NAA/Cr, NAA/Cho, Lip1.3/Cr, Lip1.3/Cho, Lip0.9/Cr, and Lip0.9/Cho ratios from OKN-007-treated group and normal rat brain. Values are represented as means ± SD. Asterisks indicate statistically significant differences (*$P < 0.05$, ***$P < 0.001$, ****$P < 0.0001$). n.s., not statistically significant; Cho, choline; Cre, creatine; Lip1.3, methylene; Lip0.9, methyl.

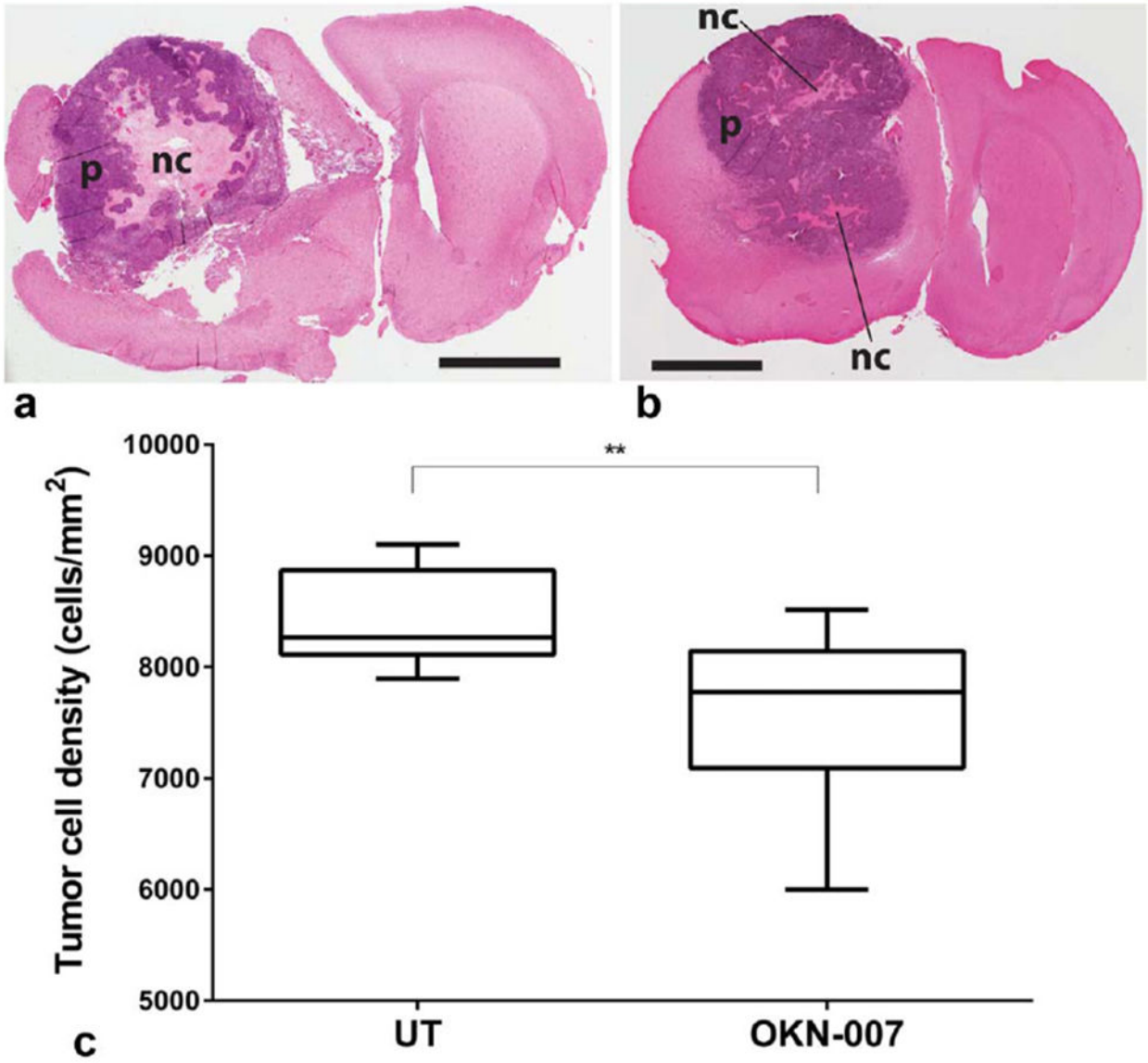

FIGURE 3:

Histological assessment of OKN-007 treatment. Representative H&E slides from UT (**A**) and OKN-007-treated (**B**) F98 gliomas. **C:** Tumor cell density (number of tumor cells/mm^2) obtained from histological sections was higher in untreated (UT) group (8442 ± 139, n = 10) than in OKN-007-treated group (7571 ± 251, n = 10). For box and whisker plot, the box extends from the 25th to 75th percentiles of tumor cell density, the line within the box is the median tumor cell density, and error bars are the minimum and maximum values. Asterisks indicate statistically significant difference (**P < 0.01). P = tumor parenchyma, and nc = tumor necrotic core. Scale bars = 3 mm.

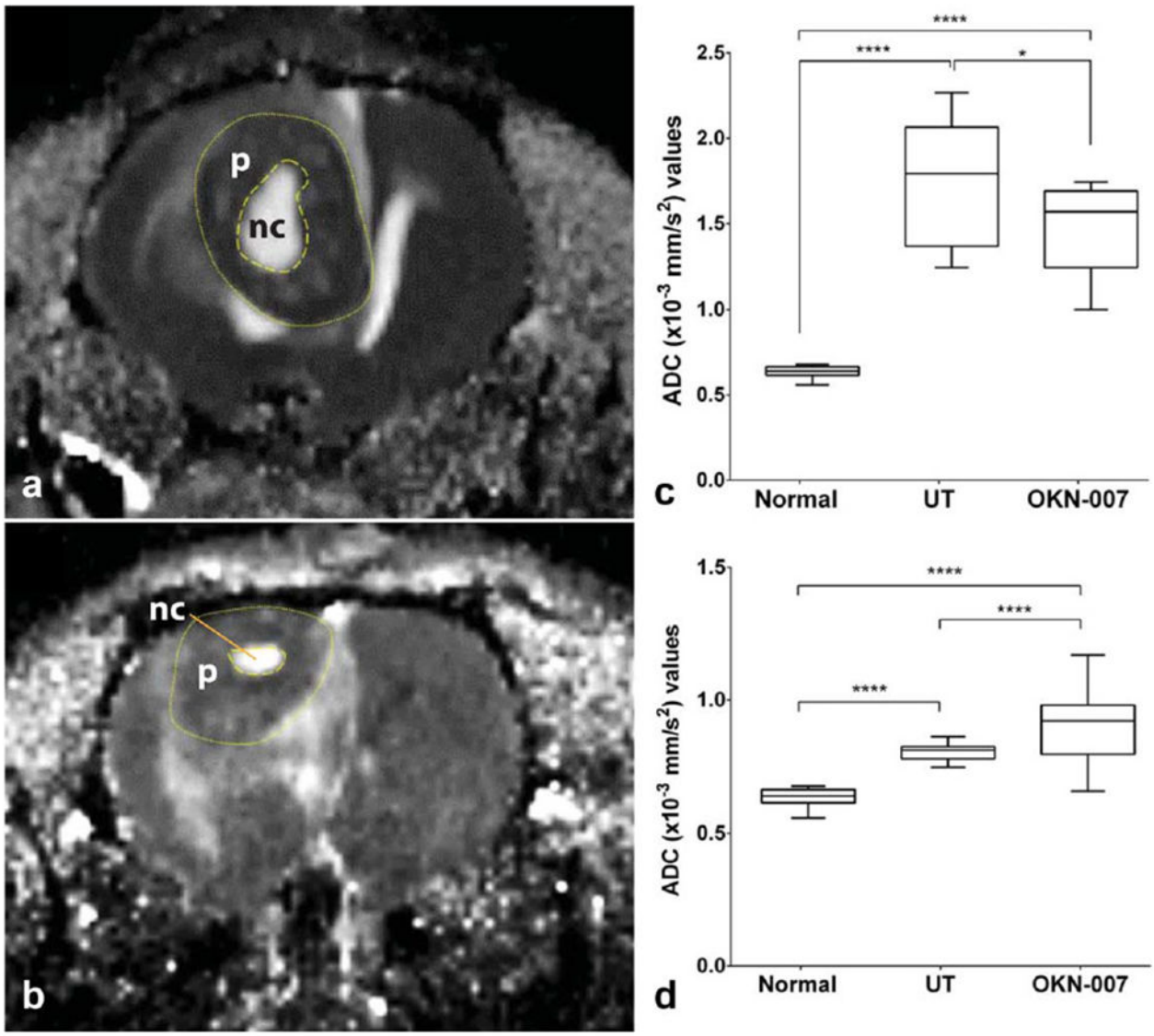

FIGURE 4:

Regional changes in ADCs after OKN-007 treatment of F98 gliomas. Representative ADC map for UT (**A**) and OKN-007-treated (**B**) F98 rat gliomas. Dashed line indicates necrotic core (hyperintense region in tumor interior) and dotted line indicates nonnecrotic tumor parenchyma (hypointense region surrounding hyperintense necrotic core). **C:** ADC values of necrotic core for OKN-treated (n = 12, >500 ROIs) group were significantly lower than in the UT group (n = 12, 529 ROIs), and both were higher than normal brain (n = 10, 30 ROIs). **D:** ADC values of nonnecrotic tumor parenchyma for OKN-treated (n = 12, >1600 ROIs) group was significantly higher compared with the UT group (n = 12, >1600 ROIs), and were both higher than normal brain (n = 10, 30 ROIs). For box and whisker plots in C and D, the box extends from the 25th to the 75th percentile of ADC values, the line within the box is the median ADC value, and error bars are the minimum and maximum ADC values. Asterisks

indicate statistically significant difference (*$P < 0.05$, ****$P < 0.0001$). P = tumor parenchyma, and nc = tumor necrotic core.

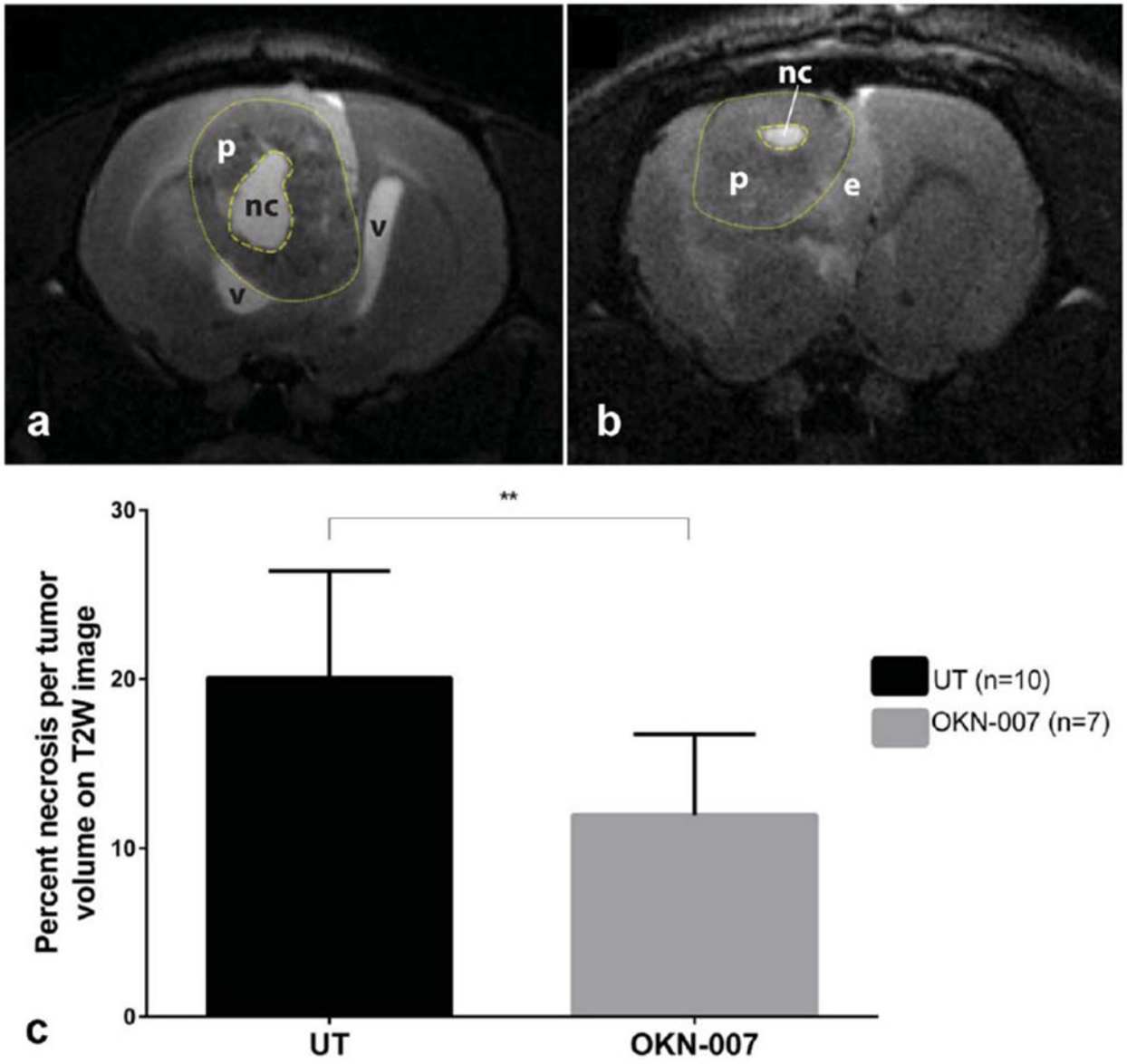

FIGURE 5:

Representative T2W images for untreated (UT) (**A**) and OKN-007-treated (**B**) F98 rat gliomas. Dashed line indicates the necrotic core (hyperintense region in tumor interior) and dotted line indicates the nonnecrotic tumor parenchyma (hypointense region surrounding hyperintense necrotic core). **C:** Percent necrosis tumor volume was significantly higher in UT group (20.08 ± 2.00, n = 10) compared with OKN-007-treated group (11.96 ± 1.80; n = 7). Values are represented as means ± SD. Asterisks indicate statistically significant difference (** $P < 0.01$). *P*, tumor periphery; nc, tumor necrotic core; v, ventricle; e, edema.

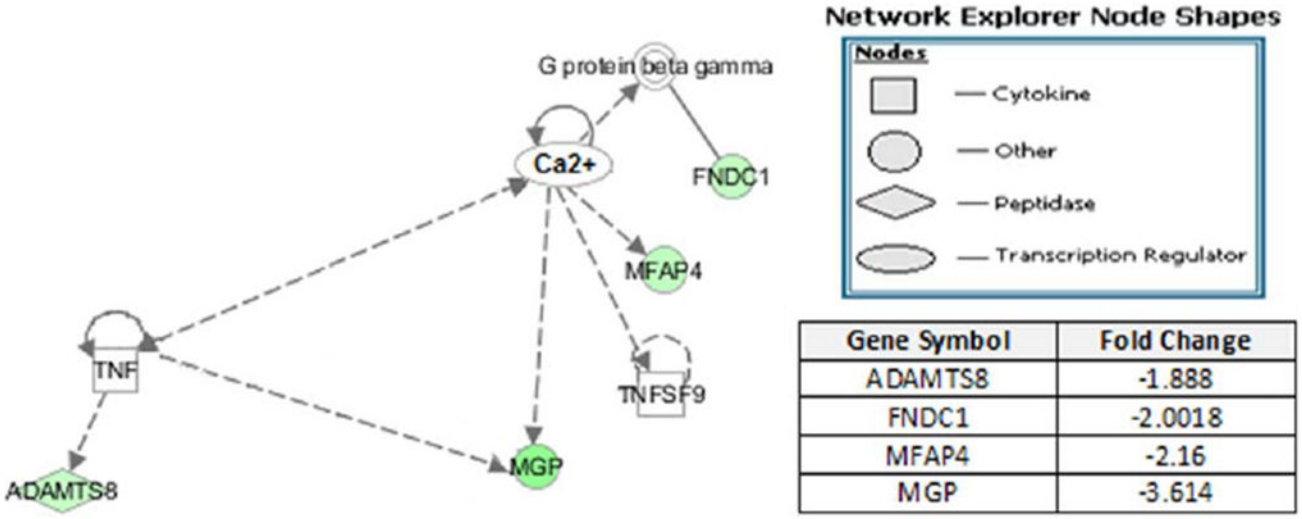

Gene Symbol	Fold Change
ADAMTS8	-1.888
FNDC1	-2.0018
MFAP4	-2.16
MGP	-3.614

FIGURE 6:

Microarray assessment of effect of OKN-007 on calcium (Ca^{2+}) channel regulation. Pathway analysis of isolated RNA from F98 gliomas that were untreated (n = 5) compared with those that were OKN-007-treated (n = 5) revealed down-regulation (depicted by a green color) in genes associated with calcium-channel regulation with a two-fold difference and 5% false discovery rate. ADAMTS8, ADAM metallopeptidase with thrombospondin type 1 motif, 8; FNDC1, fibronectin type III domain containing 1; MFAP4, microfibrillar-associated protein 4; MGP, matrix Gla protein; TNF, tumor necrosis factor; TNFSF9, tumor necrosis factor superfamily, member 9.

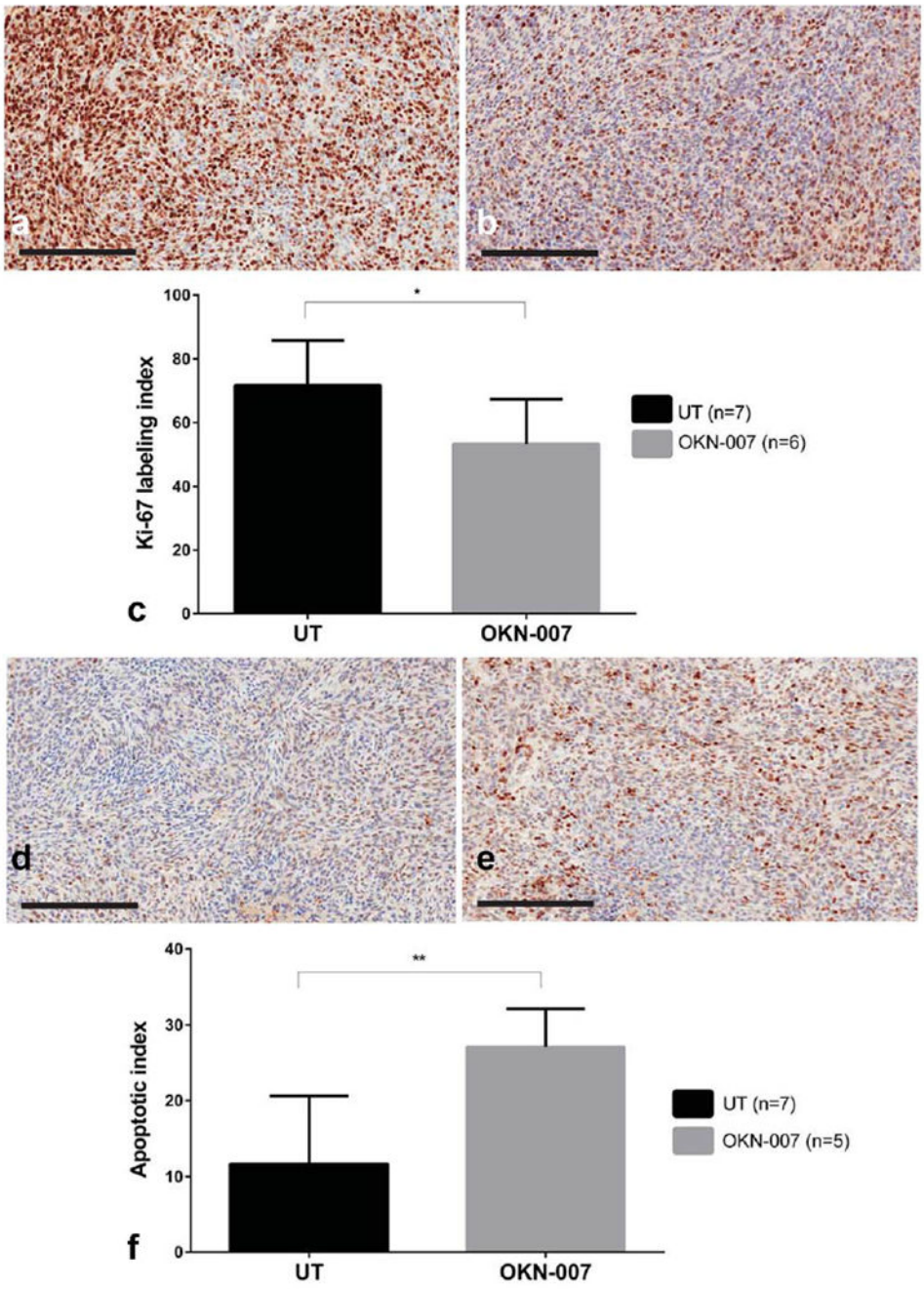

FIGURE 7:

Immunohistochemical nuclear staining of Ki-67 in an untreated (UT) (**A**) (×200) and OKN-007-treated (**B**) F98 rat glioma (×200). **C:** Ki-67 labeling index was significantly lower in OKN-007-treated group (53.25 ± 5.72, n = 6) compared with UT group (71.73 ± 5.31, n = 7). Immunohistochemical nuclear staining of cleaved caspase-3 in UT (**D**) (×200) and OKN-007-treated (**E**) F98 gliomas (×200). **F:** The apoptotic index was significantly higher OKN-007-treated (27.09 ± 2.24, n = 5) compared with UT samples

(11.69 ± 3.37, n = 7). Asterisks indicate statistically significant difference (*P<0.05, **P< 0.01). Scale bars = 200 μm.